## PAPER

# *In situ* spectroelectrochemical and theoretical study on the oxidation of a 4*H*-imidazole-ruthenium dye adsorbed on nanocrystalline TiO$_2$ thin film electrodes†

Ying Zhang,‡[ab] Stephan Kupfer,‡[a] Linda Zedler,[ab] Julian Schindler,[ab] Thomas Bocklitz,[a] Julien Guthmuller,[c] Sven Rau[d] and Benjamin Dietzek*[ab]

Terpyridine 4*H*-imidazole-ruthenium(II) complexes are considered promising candidates for use as sensitizers in dye sensitized solar cells (DSSCs) by displaying broad absorption in the visible range, where the dominant absorption features are due to metal-to-ligand charge transfer (MLCT) transitions. The ruthenium(III) intermediates resulting from photoinduced MLCT transitions are essential intermediates in the photoredox-cycle of the DSSC. However, their photophysics is much less studied compared to the ruthenium(II) parent systems. To this end, the structural alterations accompanying one-electron oxidation of the **RuIm** dye series (including a non-carboxylic **RuIm** precursor, and, carboxylic **RuImCOO** in solution and anchored to a nanocrystalline TiO$_2$ film) are investigated *via in situ* experimental and theoretical UV-Vis absorption and resonance Raman (RR) spectroelectrochemistry. The excellent agreement between the experimental and the TDDFT spectra derived in this work allows for an in-depth assignment of UV-Vis and RR spectral features of the dyes. A concordant pronounced wavelength dependence with respect to the charge transfer character has been observed for the model system **RuIm**, and both **RuImCOO** in solution and attached on the TiO$_2$ surface. Excitation at long wavelengths leads to the population of ligand-to-metal charge transfer states, *i.e.* photoreduction of the central ruthenium(III) ion, while high-energy excitation features an intra-ligand charge transfer state localized on the 4*H*-imidazole moiety. Therefore, these 4*H*-imidazole ruthenium complexes investigated here are potential multi-photoelectron donors. One electron is donated from MLCT states, and additionally, the 4*H*-imidazole ligand reveals electron-donating character with a significant contribution to the excited states of the ruthenium(III) complexes upon blue-light irradiation.

[a] *Institute of Physical Chemistry, Friedrich Schiller University Jena, Helmholtzweg 4, 07743 Jena, Germany. E-mail: benjamin.dietzek@uni-jena.de; Fax: +49-3641-948302*

[b] *Leibniz Institute of Photonic Technology Jena (IPHT), Albert-Einstein-Straße 9, 07745 Jena, Germany*

[c] *Faculty of Applied Physics and Mathematics, Gdansk University of Technology, Narutowicza 11/12, 80233 Gdansk, Poland*

[d] *Institute of Inorganic Chemistry I, University Ulm, Albert-Einstein-Allee 11, 89081 Ulm, Germany*

† Electronic supplementary information (ESI) available. See DOI: 10.1039/c5cp04484g

‡ Both authors contributed equally to this work.

## Introduction

Ruthenium polypyridyl dyes have attracted considerable interest in various applications due to their chemical stability, strong absorption of visible light, and unique redox and catalytic properties.[1–8] For example, ruthenium polypyridyl complexes are used as photosensitizers in dye-sensitized solar cells (DSSCs).

Besides the nanocrystalline semiconductor, the redox electrolyte and the platinum counter electrode the ruthenium polypyridyl complexes are one of the main components of these devices.[9,10] In DSSCs, the direct conversion of light into electrical energy occurs *via* visible light absorption by the dye molecules, followed by a generally very fast electron transfer into the wide-bandgap semiconductor.[11,12] Subsequently, the oxidized form of the adsorbed dye is re-reduced by a redox couple in the electrolyte – a process which is dominated by molecular collisions of the redox couple with the adsorbed dye.[13–15] The optimization of the performance of DSSCs is based on a detailed understanding of the system and its light-induced dynamics at a molecular level, which allows deeper insight into the structure-dynamics-function interplay in complex systems for the conversion of sunlight into electricity[16] and other storable forms of energy.[17–19] A significant amount of work focused on improving the light-absorbing properties of the sensitizer,[6,20–27] which should cover the visible range of the solar spectrum and stretch far into the IR. In this context, herein the

This journal is © the Owner Societies 2015

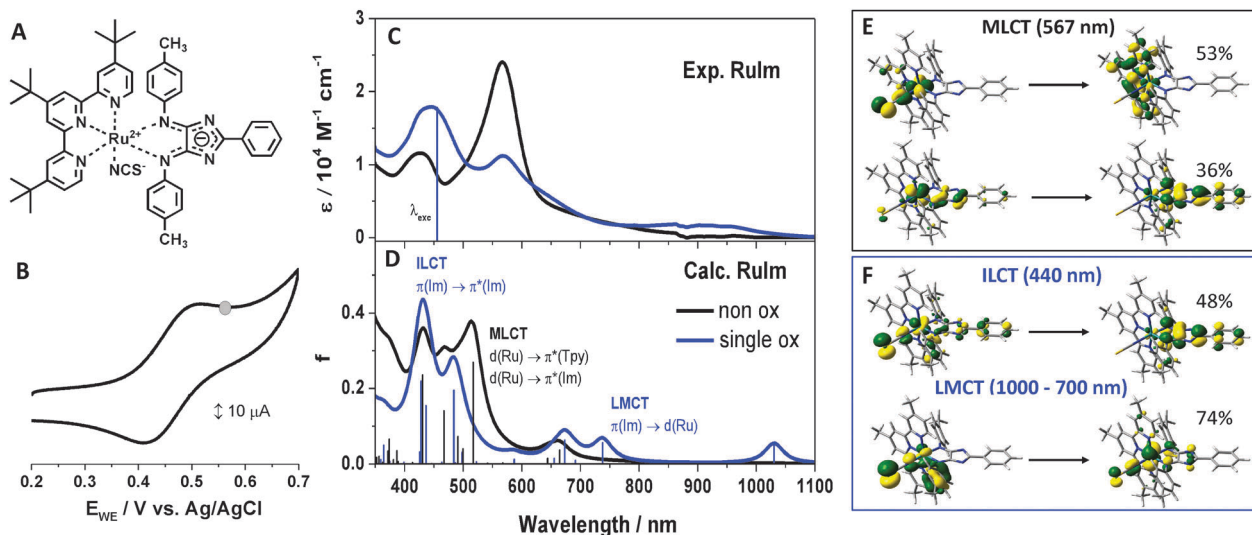*Phys. Chem. Chem. Phys.*, 2015, **17**, 29637–29646 | 29637

Fig. 1 (A) Molecular structure of **RuIm**. (B) CV obtained for the oxidation of **RuIm** in ACN with 0.1 M tetrabutylammonium tetrafluoroborate (TBABF$_4$) as supporting electrolyte with a scan rate of 50 mV s$^{-1}$, the applied oxidation potential (0.55 V vs. Ag/AgCl) during UV-Vis and RR spectroscopy is marked as a grey circle in the curve. (C) UV-Vis spectra of **RuIm** (black curve) and electrochemically oxidized **RuIm** (blue curve) in 0.1 M TBABF$_4$/ACN, with an applied potential of 0.55 V vs. Ag/AgCl. The RR excitation wavelength (458 nm) is displayed as a vertical line in the spectrum. (D) Calculated spectra of non-oxidized (black curve) and single oxidized (blue curve) **RuIm**. (E) Molecular orbitals involved in the S$_6$ MLCT transition of **RuIm**. (F) Molecular orbitals involved in the ILCT and LMCT transitions of oxidized **RuIm**.

investigated ruthenium complexes coordinating 2-phenyl-4,5-p-tolylimino-4H-imidazole (4H-imidazole) as an organic chromophore, have been introduced as panchromatic dyes.[28–30] Aside from the 4H-imidazole a polypyridyl fragment, which consists of 4,4′,4″-tri-tert-butyl-2,2′:6′,2″-terpyridine and an additional monodentate isothiocyanate ligand are coordinated to the ruthenium(II) metal center (**RuIm**) (Fig. 1A). Due to the direct and strong interaction between each chromophore with the metal center the complexes exhibit the photoelectrochemical and photophysical properties related to the ruthenium(II)-polypyridine fragment while displaying broad and strong absorption in the visible range due to the presence of strong [1]MLCT and ligand centered ([1]LC) transitions.[29–34] Furthermore, the redox and photophysical properties of the 4H-imidazole coordinating ruthenium(II) complexes can be easily tuned by varying the substituent pattern and the protonation state of the ligand, as has been recently shown.[30,31,33,34] These properties render complexes like **RuIm** with promising structures for use as molecular sensitizers in DSSCs, in which the electron injection from the photoexcited light harvesting unit into the wide bandgap semiconductor occurs via an anchoring group, typically a carboxylate group (COO$^-$).[9,35,36] High electron injection yields are obtained by placing the anchoring group close to the ligand that carries the excess charge density in the photoexcited state,[37,38] i.e., for **RuIm** at the 4H-imidazole ligand and the directly connected phenyl ring, since the lowest initially excited [1]MLCT state and the thermally relaxed [3]MLCT state, from which electron injection in the acceptor states of TiO$_2$ appears, are both dominantly localized on the imidazole fragment.[29–31,33,39] Hence, the carboxyl anchoring group has been introduced at the phenyl moiety of the 4H-imidazole ligand in order to facilitate the electronic coupling between both, the [1]MLCT and the [3]MLCT state and the acceptor

states of TiO$_2$ (**RuImCOO**, Fig. 3C). Furthermore, recently it was reported that injection for closely related complexes occurs partially from hot vibrational states, since the thermalized long-lived relaxed [3]MLCT states fall within the bandgap of TiO$_2$.[32]

In this contribution we focus on the spectroscopic properties of the photo-oxidized ruthenium(III) species of **RuImCOO**, which appear as essential mechanistic intermediates in the photoelectrochemical cycle underlying the function of the DSSC. The electronic transitions in these species, which are exposed to visible light, are studied by a combined experimental-theoretical approach utilizing UV-Vis absorption and resonance Raman (RR) spectroelectrochemistry (SEC) to study structural changes accompanying one-electron oxidation and to characterize photoexcited intermediates of the oxidized terpyridine 4H-imidazole-ruthenium(II) complexes **RuIm** and **RuImCOO** in solution. Special emphasis will be put on the identification of the predominant protonation state of the 4H-imidazole ligand sphere in **RuImCOO** since protonation strongly impacts the redox and photophysical properties of the investigated complexes. Finally, **RuImCOO** was attached to mesoporous nanocrystalline TiO$_2$ thin films and investigated by means of SEC to derive influences of the interface between the sensitizer and the semiconductor on the oxidation induced spectral shifts.

# Results and discussion

## Spectroelectrochemistry on the RuIm precursor

To aid the study and rationalization of the electronic properties of **RuImCOO** on TiO$_2$ surfaces, the complex without an anchoring group, i.e. **RuIm**, is initially studied as a benchmark system in solution. The cyclic voltammogram (CV) of **RuIm** (Fig. 1B) exhibits

a quasi-reversible oxidation peak at 0.46 V *vs.* Ag/AgCl. To gain insight into the (electronic) structures of non-oxidized and oxidized species, a combination of spectroelectrochemical UV-Vis and RR techniques is utilized.

The absorption spectrum of **RuIm** recorded in acetonitrile (ACN) exhibits two broad absorption bands in the visible region centered at 567 nm ($\varepsilon$ = 24 100 M$^{-1}$ cm$^{-1}$) and 427 nm ($\varepsilon$ = 11 600 M$^{-1}$ cm$^{-1}$) as well as a shoulder at approximately 700 nm (Fig. 1C). In order to unravel the nature of the electronic transitions underlying these absorption features quantum chemical simulations at the time-dependent density functional theory (TDDFT) level of theory have been performed (Fig. 1D and Table S1, ESI†). Based on the calculations, the first bright absorption band can be assigned to the bright $S_6$ MLCT state (517 nm) with slight contributions from the MLCT states $S_7$ (500 nm) and $S_8$ (491 nm). $S_6$ and $S_8$ feature transitions to the terpyridine as well as to the 4*H*-imidazole ligand sphere, while $S_7$ merely exhibits transitions to the terpyridine ligand. The long-wavelength shoulder at 700 nm is due to the weakly absorbing $S_1$ (664 nm, localized on the 4*H*-imizazole) and $S_2$ (644 nm, localized on the terpyridine) MLCT states. The second bright absorption band is assigned to the bright MLCT state $S_9$ (467 nm), featuring transitions towards the 4*H*-imidazole and terpyridine ligand spheres, as well as to the 4*H*-imidazole centered intra-ligand charge transfer (ILCT) state $S_{10}$. Detailed information with respect to the computational results is illustrated in Table S2 (ESI†). As predicted by TDDFT the first bright MLCT band (567 nm) is dominated by transitions to the terpyridine ligand, while transitions towards the 4*H*-imidazole feature less weight. This finding is contrary to the expectations based on the structurally closely related chloro-complex, where merely the isothiocyanate ligand is replaced by a chloro ligand.[29,34] For the previously studied chloro-complex, the first bright MLCT band is dominated by 4*H*-imidazole transitions; very similar results have been obtained for complexes with variations of the substitution pattern in the periphery of the 4*H*-imidazole.[28,33] In addition, changing the polypyridyl sphere from terpyridine to bipyridine[31,32] induces no pronounced alterations to the nature of the excited states underlying the MLCT band, hence, the majority of the MLCT transitions in the visible range involve charge density shifts towards the 4*H*-imidazole ligand. Herein the reported phenomenon of enhanced terpyridine character of the MLCT band in **RuIm** can be rationalized by means of the molecular orbital (MO) d$_{xz}$(187), which is involved in the terpyridine centered MLCT transition of the bright $S_6$ state, see Tables S1 and S2 (ESI†). In contrast to the respective MO of the chloro-complex (Fig. S1, ESI†), d$_{xz}$(187) features an increased mixing with p-orbitals of the isothiocyanate ligand. This leads in consequence to an increased weight of the terpyridine transition.

Upon electrochemical oxidation of **RuIm**, the intensity of the MLCT absorption band at 567 nm is quenched significantly, while several new absorption features arise (Fig. 1C): in the low-energy region between 1000 and 700 nm a broad yet rather weak absorption band is formed. In addition, the absorbance of the ILCT is increased substantially. This increase in absorption is accompanied by a red-shift of the band from 427 to 440 nm ($\sim$700 cm$^{-1}$) upon oxidation. Reversibility of electrochemical reduction was confirmed by measuring UV-Vis spectra during

the acquisition of a CV of oxidation (Fig. S2, ESI†). The origin of these spectral alterations is elucidated by quantum chemical calculations for the singly oxidized species of **RuIm** (Fig. 1D), where oxidation was found to be almost entirely localized on the ruthenium center (see Table S3, ESI†). The optimized equilibrium structures of both oxidation states are very similar. However, contrary to the non-oxidized singlet, the singly oxidized doublet exhibits no intense MLCT states in the visible range, which is directly correlated with the formation of the ruthenium(III) species, *i.e.*, to the decreased electron density at the ruthenium ion. Consequently, the intensity of the MLCT band is reduced in the UV-Vis-SEC measurements. Likewise, the formation of the absorption bands between 1000 and 700 nm and 440 nm can be rationalized. TDDFT assigns the low-energy band to three weakly absorbing ligand-to-metal charge transfer (LMCT) states, namely, $D_3$, $D_4$ and $D_6$ localized at 1030, 738 and 673 nm, respectively. The rising absorption band at 440 nm is due to several intense 4*H*-imidazole centered ILCT states, $D_{16}$, $D_{23}$ and $D_{31}$ at 484, 428 and 409 nm, as well as to a ligand-to-ligand charge transfer (LLCT) state from isothiocyanate to terpyridine ($D_{22}$ at 437 nm). The ILCT occurs from the terminal tolyl moieties to the central 4*H*-imidazole fragment. Thus, a pronounced wavelength dependency with respect to the charge transfer (CT) character of the electronic transitions is observed for the absorption spectrum of the oxidized **RuIm**: low-energy excitation leads to the population of LMCT states and, thus, to the formation of ruthenium(II), while high-energy excitation leads to an ILCT of the 4*H*-imidazole ligand.

In order to investigate the nature of the excited states of the non-oxidized as well as of the single oxidized **RuIm** within the respective Franck–Condon points RR-SEC has been applied.[39] For these experiments, excitation at 458 nm is employed, which is in resonance with the ILCT band centered at 427 nm (and partially with the MLCT band at 567 nm) of the non-oxidized **RuIm**.

Based on the agreement of the measured RR-SEC spectra for both redox states (Fig. 2) with the simulated RR intensity pattern (non-oxidized singlet and single oxidized doublet depicted in Fig. S3, ESI† and respective vibrational modes in Table S4, ESI†)
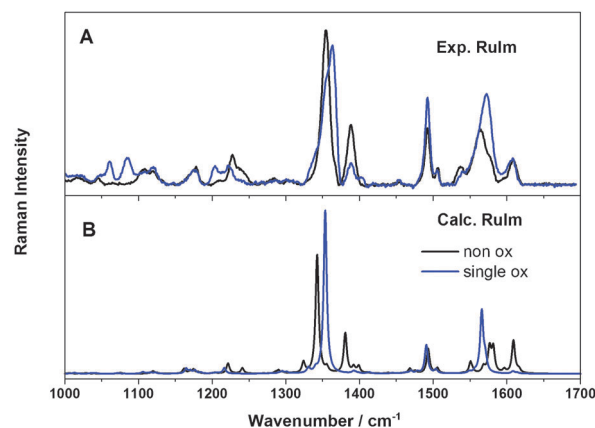


**Fig. 2** Experimental (A) and calculated (B) RR spectra for non-oxidized (black) and single oxidized (blue) **RuIm** in 0.1 M TBABF$_4$/ACN, excited at 458 nm.

almost all intense Raman bands could be assigned to vibrational normal modes. For the calculation of the RR spectrum of the non-oxidized form contributions from the MLCT states $S_6$, $S_7$, $S_8$ and $S_9$ and of the IL state $S_{10}$ have been taken into account, while the excitation energy for all states has been red-shifted by 1000 cm$^{-1}$. Following this procedure, the Raman active vibrational bands at 1226, 1240, 1354, 1388, 1492, 1505 and 1564 cm$^{-1}$ have been assigned to normal modes of the 4$H$-imidazole ligand at 1221.6, 1241.0, 1342.6, 1380.8, 1493.2, 1576.7 and 1581.7 cm$^{-1}$ (modes 163, 164, 178, 180, 205 and 207). In addition, the weak shoulders at 1340 and 1537 cm$^{-1}$ and the feature at 1609 cm$^{-1}$ have been associated with the terpyridine modes 177, 209 and 217 at 1324.0, 1550.7 and 1609.1 cm$^{-1}$, respectively. Hence, a maximum absolute deviation (MAD) of 6.9 cm$^{-1}$ is obtained for the assigned normal modes. In general contributions of the terpyridine ligand to the RR intensity pattern seem to be slightly overestimated, which correlates with the increased terpyridine character to the MLCT transition in the absorption spectrum of **RuIm**.

The excitation wavelength of 458 nm is in resonance with the rising ILCT band centered at 440 nm and the increase in intensity upon single oxidation. Consequently, alterations of the RR spectra are observed upon oxidation, *e.g.*, the most intense band (1354 cm$^{-1}$) is hypsochromically shifted by 9 cm$^{-1}$. Furthermore, the intensity of the band at 1388 cm$^{-1}$ decreases substantially, while the bands at 1492 and 1572 cm$^{-1}$ become more intense. The origin of the alteration of the RR intensity pattern is unraveled based on the simulations. Taking into account the contributions from $D_{16}$, $D_{22}$ and $D_{23}$ states and shifting the excitation energies of these states by –1000 cm$^{-1}$, an excellent agreement was achieved with respect to the frequencies as well as to the relative RR intensities (MAD of 6.9 cm$^{-1}$). Hence, the shift of the most intense resonance Raman band from 1354 to 1363 cm$^{-1}$ is reproduced by the simulations (from 1342.6 to 1353.6 cm$^{-1}$), while the underlying vibrational modes of the non-oxidized (178) and single oxidized complex (179) are assigned to 4$H$-imidazole centered modes (see Fig. S3 and Table S4, ESI†). Likewise the increase in intensity at 1492 and 1572 cm$^{-1}$ stems from contributions of the intense 4$H$-imidazole normal modes (205, 212 and 213) at 1490.8, 1566.1 and 1570.9 cm$^{-1}$. Merely the small shoulder at 1330 cm$^{-1}$ (mode 177 at 1330.7 cm$^{-1}$) is associated with the terpyridine ligand. Hence, the contribution of the terpyridine ligand sphere is considerably reduced upon single oxidation, which roots in the electronic nature of the electronic states, which are in resonance with the excitation light at 458 nm, *i.e.* intense ILCT states $D_{16}$ and $D_{23}$.

### RuImCOOH

**Effects of protonation.** It has been established that the protonation of the 4$H$-imidazole ligand fragment has a determining impact on the photophysical properties of the ligand and resulting transition metal complexes.[28–30,32,33,39] In general, protonation of ruthenium-4$H$-imidazole complexes induces a redshift of absorption due to an increased energetic stabilization of the 4$H$-imidazole π*-acceptor states.[28,29,33] Upon introduction of a carboxylic acid anchoring group at the periphery of the phenyl moiety of the 4$H$-imidazole ligand, four different protonation states are

possible: (i) **RuImCOO**, where both nitrogen atoms of the 4$H$-imidazole and the carboxylic acid group are deprotonated; (ii) **RuImCOOH**, a single protonated form with a deprotonated 4$H$-imidazole and a protonated anchoring group; (iii) **RuImHCOO**, a second single protonated form with a protonated 4$H$-imidazole and a deprotonated carboxylic acid anchoring group; and, (iv) **RuImHCOOH**, where both the bridging ligand as well as the anchoring group are protonated. Since the preparation procedure of the ruthenium(II)-terpyridine-4$H$-imidazole complex with carboxylic anchoring group leads to a partial protonation of the complex,[40] it is of major importance to identify the actual protonation state of the sample. For structurally closely related complexes a pronounced pH-dependence of the UV-Vis absorption properties has been observed.[28,29,33] In order to investigate the pH-dependent absorption properties of the carboxylic ruthenium(II)-terpyridine-4$H$-imidazole complexes, the sample was deprotonated with 1,8-diazabicyclo[5.4.0]undec-7-ene (DBU) in ACN and afterwards protonated in a step-wise manner using diluted trifluoroacetic acid (TFA).

The absorption spectrum of **RuImCOO**, depicted in Fig. S4 (ESI†), features intense bands at 570 and 442 nm and shoulders at approximately 700 and 420 nm. Thus, its absorption properties are very similar to that of the **RuIm** precursor. Upon single protonation both absorption features are bathochromically shifted to 582 ($\Delta\tilde{\nu} = -362$ cm$^{-1}$) and 451 nm ($\Delta\tilde{\nu} = -451$ cm$^{-1}$), while the absorbance of red (700 nm) and blue-sided (425 nm) shoulders decreases. Further protonation by TFA yields the double protonated species **RuImHCOOH**, whose formation is accompanied by a further red-shift of the first absorption band to 603 nm ($\Delta\tilde{\nu} = -960$ cm$^{-1}$ with respect to **RuImCOO**) and the disappearance of the red-sided shoulder. In contrast, the blue absorption band is shifted to shorter wavelengths (412 nm, $\Delta\tilde{\nu} = +1648$ cm$^{-1}$ with respect to **RuImCOO**). In order to obtain insight into the excited states underlying the absorption pattern of the protonated species TDDFT calculations have been performed within the equilibrium structures of **RuImCOO**, **RuImCOOH**, **RuImHCOO**, and **RuImHCOOH**.

The experimental results obtained for **RuImCOO** are almost identical to the data of the **RuIm** precursor, and, hence similar excited states properties are: the first absorption feature (570 nm), shown in Fig. S5 (ESI†), is assigned to the MLCT states $S_6$ (518 nm), $S_7$ (503 nm) and $S_8$ (498 nm) featuring transitions to the 4$H$-imidazole as well as to the terpyridine ligand. The second absorption band at 442 nm as well as the blue-sided shoulder (420 nm) stem from the bright $S_{10}$ (469 nm), which is a MLCT state localized on both ligand spheres, and the bright 4$H$-imidazole centered ILCT state $S_{13}$ (426 nm). Thus, the carboxylic acid anchoring group introduces only minor alterations to the excited states properties as compared to **RuIm**, which are based on its electron-withdrawing character.[5,41,42] Protonation of **RuImCOO** can result in the formation of the single protonated forms **RuImHCOO** and **RuImCOOH**, the latter of which is more stable by 4000 cm$^{-1}$. Hence, only the excited states of **RuImCOOH** are used to interpret the experimental UV-Vis data of the single protonated complex: the slight red-shift of the first absorption band upon protonation is mainly represented by the

bright MLCT state $S_6$ (532 nm) and is accompanied by a substantial increase of the 4*H*-imidazole character. Further contributions to this absorption feature originate from the weakly absorbing MLCT states $S_7$ (497 nm) and $S_8$ (490 nm). The second band (at 451 nm) and the blue-sided shoulder are assigned to the bright 4*H*-imidazole ILCT state $S_{10}$ (452 nm) and the weakly absorbing $S_9$ (468 nm) MLCT state, which is localized on the terpyridine ligand.

Double protonation leads to **RuImHCOOH**; in this protonation state the MLCT band is further shifted to higher wavelengths (*i.e.*, to 603 nm). TDDFT assigns this band to the $S_4$ MLCT state (556 nm), while the bathochromic shift is associated with a further increase of weight of the transition towards the 4*H*-imidazole. However, the blue-shift of the ILCT band upon double protonation to 412 nm is not correctly reproduced by considering the $S_6$ state (484 nm) in the quantum chemical simulation, a phenomenon which was previously reported for other 4*H*-imidazole ruthenium(II) complexes.[28,29,31–33] This problem is related to the shortcoming of TDDFT to give a balanced description for electronic states of different electronic natures, such as MLCT, IL, ILCT, and LLCT states. As shown in ref. 29 the B3LYP exchange correlation functional gives the most balanced description for the involved excited states. More detailed information concerning the computational results is presented in Tables S5–S8 of the ESI.†

In general, successive protonation from **RuImCOO** *via* **RuIm-COOH** to **RuImHCOOH** leads to a characteristic red-shift of the MLCT band, which roots in the increasing 4*H*-imidazole (and decreasing terpyridine) character of the underlying excited states. In addition, wavelength shifts have been observed for the ILCT band with respect to **RuImCOO**. Hence, the protonation state of the investigated ruthenium complex can be monitored by means of UV-Vis spectroscopy.

In the following, the protonation state of the complex is investigated upon anchoring onto the nanocrystalline $TiO_2$ film. To this end, the UV-Vis absorption of the dye anchored onto $TiO_2$ through the carboxyl group was measured in ACN (depicted in Fig. 3E and Fig. S6, ESI†). The spectrum exhibits strong absorption due to $TiO_2$ nanoparticles below 400 nm,[43] an intense MLCT absorbing band at 576 nm and a less intense 4*H*-imidazole ILCT band at 445 nm. The position of the MLCT band of the dye-sensitized $TiO_2$ film in ACN demonstrates that the 4*H*-imidazole ring is deprotonated. The comparison with the pH dependent UV-Vis spectra confirms the presence of **RuImCOO** on the dye-sensitized $TiO_2$ film. Nevertheless, both the MLCT and the ILCT band of the dye-sensitized $TiO_2$ film in ACN (at 576 and 445 nm respectively) are localized at longer wavelengths compared to the free **RuImCOO** in solution (at 570 and 442 nm, respectively). To illustrate the shifts, the UV-Vis spectra of the dye-sensitized $TiO_2$ film were also recorded under atmospheric conditions (Fig. S6, ESI†), where the spectral shape is broader than that in ACN and the intense MLCT band is bathochromically shifted to 582 nm ($\Delta\tilde{\nu} = -179$ cm$^{-1}$). These alterations indicate that the dye molecules anchored onto the $TiO_2$ film aggregate slightly and exhibit weak intermolecular interactions.[44,45] Intermolecular interactions among the dyes can be (partially) quenched by the solvent molecules (ACN) acting as spacers; however, most likely aggregation of the dyes on the surface cannot be suppressed completely. Thus, the bathochromic shifts in the UV-Vis spectra upon anchoring of **RuImCOO** onto the $TiO_2$ film are ascribed to the aggregation of the dye on the surface.

Besides UV-Vis also RR spectroscopy has been proven to be a powerful tool to discriminate different protonated states of
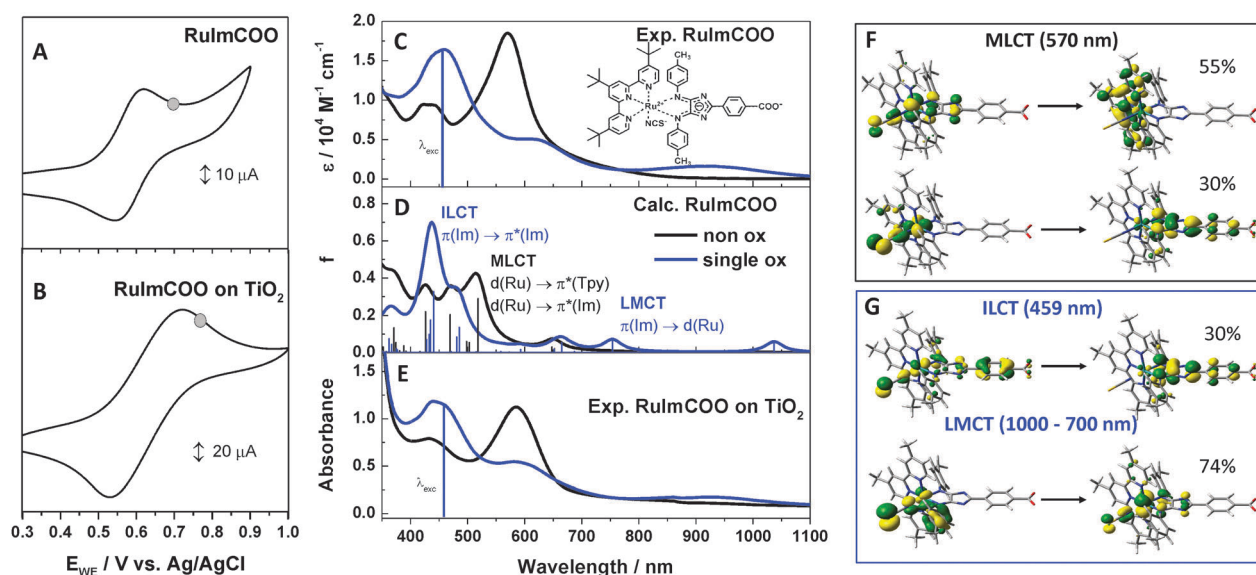


**Fig. 3** (A) and (B) CVs for the oxidation of **RuImCOO** in solution and on $TiO_2$ surface measured in 0.1 M TBABF$_4$/ACN with a scan rate of 50 mV s$^{-1}$, the applied oxidation potentials (0.70 and 0.75 V *vs.* Ag/AgCl) during UV-Vis and RR spectroscopy are marked as grey circles in the curves. (C) and (E) *In situ* UV-Vis spectra of non-oxidized **RuImCOO** (black curve) and electrochemically oxidized **RuImCOO** (blue curve) in solution and on the $TiO_2$ surface measured in 0.1 M TBABF$_4$/ACN. The RR excitation wavelength (458 nm) is displayed as a vertical line in the spectra. (D) Calculated spectra of non-oxidized (black) and single oxidized (blue) **RuImCOO** in solution. (F) Molecular orbitals involved in the $S_6$ MLCT transition of **RuImCOO** in solution. (G) Molecular orbitals involved in the ILCT and LMCT transitions of oxidized **RuImCOO** in solution.

This journal is © the Owner Societies 2015

*Phys. Chem. Chem. Phys.*, 2015, **17**, 29637–29646 | **29641**

ruthenium-polypyridyl-4H-imidazole complexes.[29,31–33] As shown in Fig. S7 (ESI†), only the double protonated species **RuImHCOOH** displays characteristic bands of the protonated 4H-imidazole ring at 1480 and 1516 cm$^{-1}$; thus the absence of these signatures further corroborates the conclusion that the dye molecule bound to TiO$_2$ is the deprotonated **RuImCOO**.

**Spectroelectrochemistry on RuImCOO in solution and on the TiO$_2$ surface.** After the identification of its protonation state, **RuImCOO** both dissolved in ACN and anchored onto a nanocrystalline TiO$_2$ film was investigated by CV and SEC. The fully reversible (single) oxidation of **RuImCOO** takes place at 0.58 V (Fig. 3A), measured vs. Ag/AgCl, and, hence, at a higher potential than the oxidation of **RuIm** (0.46 V). These results confirm that the electron withdrawing COO substituent impedes the oxidation of the ruthenium(ii) complex.[46] For **RuImCOO** on the TiO$_2$ surface, a quasi-reversible one-electron transfer process is observed (Fig. 3B), with an oxidation potential of 0.65 V vs. Ag/AgCl, which appears to be slightly higher compared to **RuImCOO** in solution due to the working electrode material (Indium-tin-oxide (ITO)[47] instead of platinum) and dye aggregation on the surface of the semiconductor.[46,48] Furthermore, a decrease in the electrical potential due to high ionic strength of the electrolyte is more pronounced during measuring the oxidation potential of the sensitizer in solution than of the sensitizer anchored to the surface of TiO$_2$, in accordance with ref. 49.

UV-Vis-SEC has been applied to study **RuImCOO** in solution as well as on the TiO$_2$ surface. Firstly, the spectral alterations of the single oxidized **RuImCOO** complex in solution are rationalized: analogous to the single oxidation of the **RuIm** precursor, oxidation of **RuImCOO** is almost entirely localized on the ruthenium atom (see Table S3, ESI†); the absorption spectrum of the oxidized species of **RuImCOO** features a significantly decreased MLCT band (570 nm) upon oxidation, while a broad absorption band arises at 459 nm; in addition, the absorbance between 1000 and 700 nm increases slightly (Fig. 3C). The slight red-shift of the absorption band with respect to **RuIm** is associated with the introduction of the electron-withdrawing carboxylic acid group. The evaluation of the excited states of the oxidized complex performed at the TDDFT level of theory enabled the assignment of these spectral alterations to specific electronic transitions (Fig. 3D). The increasing absorption between 1000 and 700 nm stems from the underlying medium bright LMCT states D$_4$, D$_7$ and D$_9$ (at 1037, 754 and 665 nm), which are associated with charge density shifts from the 4H-imidazole ligand to the central ruthenium ion. The increasing absorption band at 459 nm contains dominant contributions from the D$_{25}$, D$_{27}$, D$_{37}$, D$_{38}$ and D$_{39}$ states at 485, 481, 441, 435 and 432 nm, respectively. The ILCT states D$_{25}$ and D$_{27}$ are mainly localized on the bridging ligand, while the highly mixed D$_{37}$, D$_{38}$ and D$_{39}$ states feature LLCT and ILCT character with contributions of all three ligands. Hence, low-energy excitation leads to the direct population of LMCT states and, thus, to a photoreduction of ruthenium(iii). On the other hand, excitation under blue light leads to an ILCT towards the central moiety of the 4H-imidazole.

The UV-Vis-SEC of **RuImCOO** on the TiO$_2$ surface resembles the respective data in solution with increasing LMCT and ILCT bands and a decreasing MLCT band (Fig. 3E). Therefore, oxidized

**RuImCOO** on the TiO$_2$ surface also shows the same wavelength dependence of the CT features; with low-energy excitation yielding ruthenium(ii) and high-energy excitation leading to an ILCT located on the 4H-imidazole ligand. Hence, anchoring onto nanocrystalline TiO$_2$ does not affect the photophysical properties of the dye significantly.

In order to investigate the potential applications of **RuImCOO** as sensitizers in DSSCs, RR-SEC has been applied to study the photophysical properties of the excited states. These measurements have been performed for the complex bound to the TiO$_2$ surface as well as in solution with an excitation wavelength of 458 nm, while the quantum chemical simulations – due to the complexity associated with the inclusion of the semiconductor surface – have been carried out exclusively for **RuImCOO** in solution. Hence, at first the RR-SEC data for the complex on TiO$_2$ will be discussed. The RR spectrum of the non-oxidized **RuImCOO** on the TiO$_2$ film features intense Raman bands at 1356, 1392, 1502, 1568 and 1607 cm$^{-1}$ as well as weak bands and shoulders at 1227, 1477, 1517 and 1537 cm$^{-1}$ (Fig. 4A). Analogous to **RuIm**, the bands at 1227, 1356, 1392, 1502 and 1568 cm$^{-1}$ are assigned to vibrational normal modes of the 4H-imidazole ligand (normal mode displacements of the respective modes are summarized in the ESI†), and the other bands at 1477 and 1607 cm$^{-1}$ are associated with the terpyridine ligand (see Tables S4 and S9, ESI†). Upon electrochemical oxidation of the dye-sensitized TiO$_2$ film, the intense bands at 1356 and 1568 cm$^{-1}$ are slightly shifted to higher frequencies, i.e. to 1359 and 1576 cm$^{-1}$. Furthermore, the band at 1392 cm$^{-1}$ decreases upon oxidation, while the weak RR signals and shoulders arise at 1336, 1517 and 1478 cm$^{-1}$. Likewise the most intense bands (i.e., at 1359, 1502 and 1576 cm$^{-1}$) are correlated with normal modes associated with the 4H-imidazole ligand. Hence, the contribution of the 4H-imidazole ligand is considerable for both the non-oxidized and oxidized anchored **RuImCOO**.

The RR spectrum of the non-oxidized **RuImCOO** in solution is illustrated in Fig. 4B and features intense Raman bands at 1356, 1389, 1496 and 1567 cm$^{-1}$ as well as less intense bands and shoulders at 1227, 1328, 1504, 1537 and 1609 cm$^{-1}$. Based on the computed RR intensity pattern (Fig. 4C) which takes into account contributions from the excited states S$_6$, S$_{10}$, and S$_{13}$, the respective excitations energies have been slightly red-shifted by 1000 cm$^{-1}$ (Fig. S8 and Table S9, ESI†). Almost all bands could be assigned to vibrational normal modes with a MAD of 8.4 cm$^{-1}$. All RR signals besides the weak bands at 1537 and 1609 cm$^{-1}$ and the shoulders at 1328 and 1504 cm$^{-1}$ are assigned to vibrational normal modes of the 4H-imidazole ligand. Upon single oxidation the intense 4H-imidazole bands at 1356, 1496 and 1567 cm$^{-1}$ are slightly shifted to higher frequencies at 1359, 1502 and 1571 cm$^{-1}$, while the formation of the weak RR signals (and shoulders) at 1336, 1402, 1478 and 1540 cm$^{-1}$ is assigned to vibrational modes localized on the terpyridine ligand. Analogous to the procedure for the oxidized **RuIm**, the energies of the states contributing to the RR intensity pattern (D$_{25}$, D$_{27}$, D$_{37}$, D$_{38}$ and D$_{39}$) have been blue-shifted by 1000 cm$^{-1}$. A comparison of the RR-SEC spectra of the anchored complex **RuImCOO** and **RuImCOO** in solution yields merely minor alterations of the RR intensity pattern. Thus, the
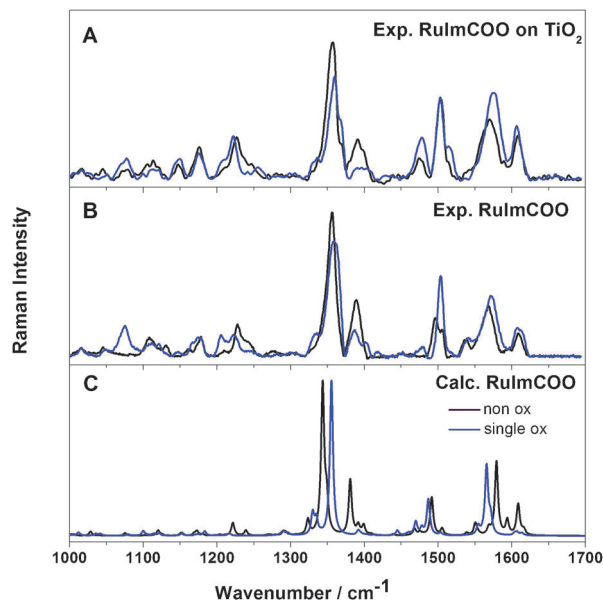
29642 | Phys. Chem. Chem. Phys., 2015, **17**, 29637–29646

This journal is © the Owner Societies 2015

Fig. 4 (A) RR spectra of non-oxidized (black) and oxidized (blue) **RuImCOO** on TiO$_2$ film, immersed in 0.1 M TBABF$_4$/ACN; (B) and (C) Experimental and calculated RR spectra of non-oxidized (black) and oxidized (blue) **RuImCOO** in solution, measured in 0.1 M TBABF$_4$/ACN; all the excitation wavelengths were 458 nm.

excited states in both **RuImCOO** systems (on TiO$_2$ and in solution) are centered on the 4$H$-imidazole ligand.

Hence, as shown by UV-Vis-SEC, RR-SEC in combination with quantum chemical simulations the oxidized **RuImCOO** both on TiO$_2$ and in solution features an ILCT state localized on the 4$H$-imidazole upon blue-light irradiation, while photoexcitation with red light leads to the regeneration of the ruthenium(II) species.

# Experimental section

## Sample preparation

The complexes **RuIm** and **RuImCOOH** were provided by Prof. Rau.[40] All samples were dissolved in anhydrous ACN (Sigma-Aldrich, spectroscopic grade), which was dried using calcium hydride (Sigma-Aldrich, 98%) and distilled twice. Dye solutions were prepared with a concentration of 0.25 mM in ACN. To obtain the non-protonated **RuIm** complex, additional traces of DBU (Sigma-Aldrich, 98%) were added into the solution to deprotonate the sample which is partly protonated due to the preparation procedure.[40] Protonation and deprotonation states of **RuImCOOH** were adjusted by addition of aliquots of 0.02 M TFA (Sigma-Aldrich, >99.5%) and DBU. 0.1 mM TBABF$_4$ in ACN was used as an electrolyte for the electrochemical and spectroelectrochemical experiments. Nanocrystalline and transparent TiO$_2$ films were prepared according to Kallioinen et al.[50] from diluted anatase paste (Ti-Nanoxide HT) consisting of 8–10 nm diameter TiO$_2$ particles (Solaronix SA, Switzerland). The paste was spread on a 1 mm thick, 7 mm width ITO glass slide. After drying at room temperature, the slide was calcined at 450 °C for 15 min and then cooled off slowly. Afterwards the film

was stained in a dye bath containing 0.5 mM **RuImCOOH** in ACN for about 16 hours. After sensitization of the TiO$_2$, physisorbed dye was wiped off by purging the film with ACN. All measurements were carried out just directly after the preparation of the films to minimize the effect of aging of the samples.

## Spectroscopic measurements

UV-Vis spectra were recorded on a double-beam Cary 5000 UV-Vis spectrometer (Varian, USA) at room temperature. RR experiments were performed through excitation by the visible lines of an Innova 300C Argon ion laser (Coherent, USA) and detected using an Acton SpectraPro 2758i spectrometer (Princeton Instruments, USA) with an entrance slit width of 100 μm, focal length 750 mm, and grating 1800 Blz/500 nm. The Raman signals were recorded using a liquid-nitrogen-cooled SPEC-10 CCD detector (Princeton Instruments, USA). The Raman spectra were subjected to a SNIP baseline correction.[51] The iteration parameter was set to 37 and pre-smoothing was applied to allow for an adaptive baseline estimate, which is not prone to noise artefacts. The ACN solvent spectrum was subtracted from all RR spectra.

UV-Vis-SEC, RR-SEC and CV measurements were performed either in a three-electrode thin-layer spectroelectrochemical cell with a pathlength of 1 mm (Bioanalytical Systems, USA), for the measurement of free dye in solution, or in a standard 5 mm pathlength cuvette, for the measurement on the TiO$_2$ film. The three-electrode system contains a Pt counter electrode, an Ag/AgCl pseudo-reference electrode and either a Pt-gauze working electrode or a dye-sensitized TiO$_2$ film on ITO glass. The potential was adjusted using a PC-controlled potentiostat. The potentials were measured with respect to the Ag/AgCl reference electrode, against which the oxidation of ferrocene was measured to be +0.42 V under the same experimental conditions. CVs were obtained at a scan rate of 50 mV s$^{-1}$. The insulating properties of nanocrystalline TiO$_2$ films in the probe potential range provide a background free platform for monitoring the oxidation reactions of adsorbed dye molecules. The spectra of the oxidized dye were taken after a certain time until the spectra remain constant, allowing for saturation of the dye oxidation processes. UV-Vis and RR spectra were recorded before and after each spectroelectrochemical measurement to check the quality and stability of the samples.

## Computational details

In order to reduce the computational cost of the simulations without affecting the spectroscopic properties of the complexes, the three *tert*-butyl groups of the terpyridine ligand have been approximated in the calculations by methyl groups. The structural and electronic data for the **RuIm** precursor as well as for the respective complex featuring a carboxylic acid anchoring group in the deprotonated (**RuImCOO**), single protonated (**RuImCOOH** and **RuImHCOO**) and double protonated form (**RuImHCOOH**) were obtained from quantum chemical simulations performed using the Gaussian 09 program.[52] All complexes have been investigated in their non-oxidized singlet form, while **RuIm** and **RuImCOO** have been studied additionally as single oxidized doublets. The geometries, vibrational frequencies and normal

This journal is © the Owner Societies 2015

Phys. Chem. Chem. Phys., 2015, **17**, 29637–29646 | 29643

coordinates of the electronic ground state (non-oxidized: singlet, single oxidized: doublet) were calculated at the density functional theory level of theory using the B3LYP[53,54] exchange–correlation functional and employing the 6-31G(d) double-$\zeta$ basis set[55] for all main group elements. For the ruthenium atom the 28-electron relativistic core potential MWB[56] was applied with its basis set describing the valence electrons (4s, 4p, 4d and 5s) explicitly and the inner shells by means of a core potential. In order to correct for the lack of anharmonicity and the approximate treatment of electron correlation the harmonic vibrational frequencies were scaled by a factor of 0.97.[57] The vertical excitation energies, oscillator strengths and analytic Cartesian energy derivatives of the excited states were obtained by TDDFT within the adiabatic approximation and by utilizing the same exchange–correlation functional, basis set and pseudopotential. As shown in ref. 28 and 29, B3LYP provides the most balanced description of the absorption features for this class of complexes.

The simulated absorption spectra have been determined based on the excitation energies and oscillator strengths of the 120 lowest excited states of the respective ground state multiplicity. The integral equation formalism of the polarizable continuum model[58] was applied to take interactions with a solvent (ACN: $\varepsilon = 35.688$, $n = 1.344$) into account with respect to the equilibrium geometry, vibrational frequencies, excitation energies, transition dipole moments and excited state gradients. For the calculations of the excitation energies and excited state gradients, where only the fast reorganization of the solvent is important, the non-equilibrium procedure of solvation was used.

The RR spectra have been calculated within the independent mode displace harmonic oscillator model (IMDHOM) assuming that the electronic ground and excited states potentials are harmonic oscillators and merely displaced in the equilibrium position and, hence, share the same set of vibrational modes.[59,60] Detailed information with respect to the computational method can be found in ref. 39 and 61 and the references therein.

In order to calculate the RR intensities of the present ruthenium complexes upon excitation at 458 nm a dumping factor of $\Gamma = 1500$ cm$^{-1}$ describing homogeneous broadening was assumed in the simulations to reproduce the experimental broadening.

The RR intensity pattern for the non-oxidized form of **RuIm** has been simulated by taking into account contributions from the S$_6$, S$_7$, S$_8$, S$_9$ and S$_{10}$, while all excitation energies have been shifted by $-1000$ cm$^{-1}$. The respective RR spectrum of the oxidized form was obtained based on the excited doublet states D$_{16}$, D$_{22}$ and D$_{23}$, which have been hypsochromically shifted by 1000 cm$^{-1}$. Likewise a shift of 1000 cm$^{-1}$ has been applied for the S$_6$, S$_{10}$ and S$_{13}$ states of the non-oxidized **RuImCOO** and of $-1000$ cm$^{-1}$ for the D$_{25}$, D$_{37}$, D$_{38}$ and D$_{39}$ of the single oxidized doublet. To reproduce the RR intensity pattern for the non-oxidized single and double protonated forms the excitation energies of the states S$_6$, S$_7$, S$_8$, S$_9$ and S$_{10}$ of **RuImCOOH** and S$_4$, S$_6$, S$_{11}$ and S$_{12}$ of **RuImHCOOH** have been bathochromically shifted by 1000 cm$^{-1}$.

The baseline estimation of the experimental Raman spectra was carried out applying the statistical language R[62] using the 'peaks' package.[63]

## Conclusion

A joint theoretical-experimental SEC study on the oxidation of black absorbing dyes was reported. The photophysical and photochemical properties of the precursors **RuIm** and **RuImCOO** as well as their photoexcited intermediates have been studied by using UV-Vis-SEC and RR-SEC methods. In addition, alterations of the spectroscopic properties of **RuImCOO** upon anchoring onto nanocrystalline TiO$_2$ have been investigated. Consequently, a concordant pronounced wavelength dependency with respect to the CT character has been determined for **RuIm**, the soluted **RuImCOO** and **RuImCOO** on the TiO$_2$ surface, that is, low-energy excitation leads to the population of LMCT states, thus yields the formation of ruthenium(ii), while high-energy excitation localizes the excited state in the 4$H$-imidazole ligand. Therefore, these 4$H$-imidazole ruthenium complexes are potential multi-photo-electron donors: one electron is donated from MLCT states, and additionally, the 4$H$-imidazole ligand reveals electron-donating character with a significant contribution to the excited states of the ruthenium(iii) complexes upon blue-light irradiation. Future measurements will aim at the determination of the photon to electron conversion efficiency (IPCE) since those experiments would provide information about the potential of 4$H$-imidazole complexes as multi-photoelectron donors in dye-sensitized solar cells.

## Acknowledgements

## Notes and references

1 S. Campagna, F. Puntoriero, F. Nastasi, G. Bergamini and V. Balzani, in *Photochemistry and Photophysics of Coordination Compounds I SE - 133*, ed. V. Balzani and S. Campagna, Springer, Berlin Heidelberg, 2007, vol. 280, pp. 117–214.
2 V. Balzani and A. Juris, *Coord. Chem. Rev.*, 2001, **211**, 97–115.
3 H.-W. Tseng, R. Zong, J. T. Muckerman and R. Thummel, *Inorg. Chem.*, 2008, **47**, 11763–11773.
4 C. Busche, P. Comba, A. Mayboroda and H. Wadepohl, *Eur. J. Inorg. Chem.*, 2010, 1295–1302.
5 A. Islam, H. Sugihara and H. Arakawa, *J. Photochem. Photobiol., A*, 2003, **158**, 131–138.
6 A. Hagfeldt, G. Boschloo, L. Sun, L. Kloo and H. Pettersson, *Chem. Rev.*, 2010, **110**, 6595–6663.
7 A. J. Esswein and D. G. Nocera, *Chem. Rev.*, 2007, **107**, 4022–4047.
8 A. J. Morris, G. J. Meyer and E. Fujita, *Acc. Chem. Res.*, 2009, **42**, 1983–1994.
9 B. O'Regan and M. Gratzel, *Nature*, 1991, **353**, 737–740.
10 M. Gratzel, *Nature*, 2001, **414**, 338–344.

29644 | *Phys. Chem. Chem. Phys.*, 2015, **17**, 29637–29646

This journal is © the Owner Societies 2015

11 J.-K. Lee and M. Yang, *Mater. Sci. Eng., B*, 2011, **176**, 1142–1160.

12 L. J. Antila, P. Myllyperkiö, S. Mustalahti, H. Lehtivuori and J. Korppi-Tommola, *J. Phys. Chem. C*, 2014, **118**, 7772–7780.

13 G. Boschloo and A. Hagfeldt, *Acc. Chem. Res.*, 2009, **42**, 1819–1826.

14 E. A. Gibson, L. Le Pleux, J. Fortage, Y. Pellegrin, E. Blart, F. Odobel, A. Hagfeldt and G. Boschloo, *Langmuir*, 2012, **28**, 6485–6493.

15 T. Daeneke, A. J. Mozer, T.-H. Kwon, N. W. Duffy, A. B. Holmes, U. Bach and L. Spiccia, *Energy Environ. Sci.*, 2012, **5**, 7090–7099.

16 S. Ardo and G. J. Meyer, *Chem. Soc. Rev.*, 2009, **38**, 115–164.

17 L. Sun, L. Hammarström, B. Åkermark and S. Styring, *Chem. Soc. Rev.*, 2001, **30**, 36–49.

18 A. Magnuson, M. Anderlund, O. Johansson, P. Lindblad, R. Lomoth, T. Polivka, S. Ott, K. Stensjö, S. Styring, V. Sundström and L. Hammarström, *Acc. Chem. Res.*, 2009, **42**, 1899–1909.

19 D. Gust, T. A. Moore and A. L. Moore, *Acc. Chem. Res.*, 2009, **42**, 1890–1898.

20 C.-Y. Chen, M. Wang, J.-Y. Li, N. Pootrakulchote, L. Alibabaei, C. Ngoc-le, J.-D. Decoppet, J.-H. Tsai, C. Grätzel, C.-G. Wu, S. M. Zakeeruddin and M. Grätzel, *ACS Nano*, 2009, **3**, 3103–3109.

21 P. Wang, S. M. Zakeeruddin, J. E. Moser, R. Humphry-Baker, P. Comte, V. Aranyos, A. Hagfeldt, M. K. Nazeeruddin and M. Grätzel, *Adv. Mater.*, 2004, **16**, 1806–1811.

22 D. Kuang, S. Ito, B. Wenger, C. Klein, J.-E. Moser, R. Humphry-Baker, S. M. Zakeeruddin and M. Grätzel, *J. Am. Chem. Soc.*, 2006, **128**, 4146–4154.

23 N. Robertson, *Angew. Chem., Int. Ed.*, 2006, **45**, 2338–2345.

24 M. K. Nazeeruddin, P. Pechy and M. Grätzel, *Chem. Commun.*, 1997, 1705–1706.

25 Y. Ooyama and Y. Harima, *Eur. J. Org. Chem.*, 2009, 2903–2934.

26 A. Mishra, M. K. R. Fischer and P. Bäuerle, *Angew. Chem., Int. Ed.*, 2009, **48**, 2474–2499.

27 S. Altobello, R. Argazzi, S. Caramori, C. Contado, S. Da Fré, P. Rubino, C. Choné, G. Larramona and C. A. Bignozzi, *J. Am. Chem. Soc.*, 2005, **127**, 15342–15343.

28 M. Wächtler, S. Kupfer, J. Guthmuller, S. Rau, L. González and B. Dietzek, *J. Phys. Chem. C*, 2012, **116**, 25664–25676.

29 S. Kupfer, J. Guthmuller, M. Wächtler, S. Losse, S. Rau, B. Dietzek, J. Popp and L. González, *Phys. Chem. Chem. Phys.*, 2011, **13**, 15580–15588.

30 M. Wächtler, M. Maiuri, D. Brida, J. Popp, S. Rau, G. Cerullo and B. Dietzek, *ChemPhysChem*, 2013, **14**, 2973–2983.

31 S. Kupfer, M. Wächtler, J. Guthmuller, J. Popp, B. Dietzek and L. González, *J. Phys. Chem. C*, 2012, **116**, 19968–19977.

32 J. Schindler, S. Kupfer, M. Wächtler, J. Guthmuller, S. Rau and B. Dietzek, *ChemPhysChem*, 2015, **16**, 1061–1070.

33 M. Wächtler, S. Kupfer, J. Guthmuller, J. Popp, L. González and B. Dietzek, *J. Phys. Chem. C*, 2011, **115**, 24004–24012.

34 L. Zedler, S. Kupfer, I. R. de Moraes, M. Wächtler, R. Beckert, M. Schmitt, J. Popp, S. Rau and B. Dietzek, *Chem. – Eur. J.*, 2014, **20**, 3793–3799.

35 G. J. Meyer, *Inorg. Chem.*, 2005, **44**, 6852–6864.

36 C. Pérez León, L. Kador, B. Peng and M. Thelakkat, *J. Phys. Chem. B*, 2006, **110**, 8723–8730.

37 K. J. Young, L. A. Martini, R. L. Milot, R. C. Snoeberger III, V. S. Batista, C. A. Schmuttenmaer, R. H. Crabtree and G. W. Brudvig, *Coord. Chem. Rev.*, 2012, **256**, 2503–2520.

38 K. Sayama, S. Tsukagoshi, T. Mori, K. Hara, Y. Ohga, A. Shinpou, Y. Abe, S. Suga and H. Arakawa, *Sol. Energy Mater. Sol. Cells*, 2003, **80**, 47–71.

39 M. Wächtler, J. Guthmuller, L. González and B. Dietzek, *Coord. Chem. Rev.*, 2012, **256**, 1479–1508.

40 S. Losse, *Redoxaktive metallorganische Farbstoffkomplexe zur Verwendung in Photovoltaik und Photokatalyse*, Diss. Friedrich-Schiller-Universität Jena, 2010.

41 M. K. Nazeeruddin, S. M. Zakeeruddin, R. Humphry-Baker, M. Jirousek, P. Liska, N. Vlachopoulos, V. Shklover, C.-H. Fischer and M. Grätzel, *Inorg. Chem.*, 1999, **38**, 6298–6305.

42 E. Badaeva, V. V. Albert, S. Kilina, A. Koposov, M. Sykora and S. Tretiak, *Phys. Chem. Chem. Phys.*, 2010, **12**, 8902–8913.

43 M. M. Ba-Abbad, A. A. H. Kadhum, A. B. Mohamad, M. S. Takriff and K. Sopian, *Int. J. Electrochem. Sci.*, 2012, **7**, 4871–4888.

44 R. Katoh, A. Furube, M. Kasuya, N. Fuke, N. Koide and L. Han, *J. Mater. Chem.*, 2007, **17**, 3190–3196.

45 M. Murai, A. Furube, M. Yanagida, K. Hara and R. Katoh, *Chem. Phys. Lett.*, 2006, **423**, 417–421.

46 A. Ehret, L. Stuhl and M. T. Spitler, *J. Phys. Chem. B*, 2001, **105**, 9960–9965.

47 M. Choi, K. Jo and H. Yang, *Bull. Korean Chem. Soc.*, 2013, **34**, 421–425.

48 J. R. Lenhard and B. R. Hein, *J. Phys. Chem.*, 1996, **100**, 17287–17296.

49 E. J. F. Dickinson, J. G. Limon-Petersen, N. V Rees and R. G. Compton, *J. Phys. Chem. C*, 2009, **113**, 11157–11171.

50 J. Kallioinen, G. Benkö, P. Myllyperkiö, L. Khriachtchev, B. Skårman, R. Wallenberg, M. Tuomikoski, J. Korppi-Tommola, V. Sundström and A. P. Yartsev, *J. Phys. Chem. B*, 2004, **108**, 6365–6373.

51 C. G. Ryan, E. Clayton, W. L. Griffin, S. H. Sie and D. R. Cousens, *Nucl. Instrum. Methods Phys. Res., Sect. B*, 1988, **34**, 396–402.

52 M. J. Frisch, G. W. Trucks, H. B. Schlegel, G. E. Scuseria, M. A. Robb, J. R. Cheeseman, G. Scalmani, V. Barone, B. Mennucci and G. A. Petersson, *et al.*, Gaussian 09, Revision A.1, Gaussian, Inc., Wallingford CT, 2009.

53 A. D. Becke, *J. Chem. Phys.*, 1993, **98**, 5648–5652.

54 C. Lee, W. Yang and R. G. Parr, *Phys. Rev. B: Condens. Matter Mater. Phys.*, 1988, **37**, 785.

55 P. C. Hariharan and J. A. Pople, *Theor. Chim. Acta*, 1973, **28**, 213–222.

56 D. Andrae, U. Haeussermann, M. Dolg, H. Stoll and H. Preuss, *Theor. Chim. Acta*, 1990, **77**, 123–141.

57 J. P. Merrick, D. Moran and L. Radom, *J. Phys. Chem. A*, 2007, **111**, 11683–11700.

This journal is © the Owner Societies 2015

*Phys. Chem. Chem. Phys.*, 2015, **17**, 29637–29646 | 29645

58 B. Mennucci, C. Cappelli, C. A. Guido, R. Cammi and J. Tomasi, *J. Phys. Chem. A*, 2009, **113**, 3009–3020.

59 J. B. Page and D. L. Tonks, *J. Chem. Phys.*, 1981, **75**, 5694–5708.

60 W. L. Peticolas and T. Rush, *J. Comput. Chem.*, 1995, **16**, 1261–1270.

61 J. Guthmuller and L. González, *Phys. Chem. Chem. Phys.*, 2010, **12**, 14812–14821.

62 R Core Team, *R: A Language and Environment for Statistical Computing*, R Foundation for Statistical Computing, Vienna, Austria, 2014.

63 M. Morhac, *Peaks: Peaks, R package version 0.2*, 2012.